Indian Journal of Chemical Technology
Vol. 24, March, 2017 pp. 184-191

Mechanical and morphological properties of halloysite nanotubes filled ethylene-vinyl acetate copolymer nanocomposites

Suvendu Padhi[1] , P Ganga Raju Achary[1] & Nimai C Nayak*[,2]

[1]Department of Chemistry, Siksha 'O' Anusandhan University, Bhubaneswar 751 030, Odisha, India.
[2] Center for Nanoscience and Nanotechnology, Siksha 'O' Anusandhan University, Bhubaneswar 751 030, India.

E-mail: nimainayak@soauniversity.ac.in

Received 14 September 2015; accepted 17 October 2016

The EVA/HNTs nanocomposites have been synthesized by solution casting technique with 0, 2.5, 5.0, 7.5 and 10 phr HNTs loading. The mechanical properties, thermal decomposition, dynamic mechanical properties of these nanocomposites are reported. The scorch time, cure time and maximum torque increases marginally on the loading of HNTs; however the curing rate index decreases. The interactions between EVA matrix and filler HNTs are evaluated by the Fourier transform infrared spectroscopy (FTIR) study. The SEM images of cryogenically fractured EVA/HNTs nanocomposites show that the roughness of the fracture surface increases with the increase in HNTs loading. The effects of HNTs loading on tensile strength, elongation break and tensile modulus of these nanocomposites have also been reported. The tensile strength and elongation break of nanocomposites increases with increase in HNTs loading up to 5phr and afterwards a decreasing trend is observed. The tensile modulus shows an increasing trend up to 5phr and decreases up to 7.5phr HNTs loading. The good dispersion of HNTs into the EVA matrix is validated by SEM analysis. The tan δ_{max} values of nanocomposites decreases up to 5phr HNTs loading and then increases which may be due to filler-filler interaction at higher HNTs loading.

Keywords: Polymer nanocomposites (PNC), Ethylene-vinyl acetate copolymers (EVA), Halloysite nanotubes (HNTs), Solution casting, TGA, DMA

Polymer nanocomposites (PNCs) containing inorganic fillers have attracted, more interest in academic and industrial fields due to the nanoparticle's unique characteristics, including their large surface area, high surface reactivity, and relatively low cost[1]. Conventional nanofillers like carbon black, graphite, silica, and silicate can enhance numerous polymer properties, generating increased mechanical properties, improved thermal resistance, and reduced gas permeability. The recent problem which has been proposed by many researchers is to replace the conventional fillers like carbon black and silica with new fillers[2]. Carbon black (CB) is good reinforcement filler with good dispersibility in the matrix due to its hydrophobic surface and particles special shape[3]. Carbon black causes pollution, more expensive and display dark colour[4,5]. So a new type of fillers such as clay minerals was introduced by researchers[5-8] to improve the physico-mechanical properties of polymer materials. Clay minerals are most potential nanoscale additives due to their 1nm thick planar structures of layers. The large aspect ratio, high strength, and relatively low density of one dimension tube-like nanofillers have attracted much interest in research[9,10].

In this study, halloysite nanotubes (HNTs) used as nanofiller is a natural occurring clay mineral and are mined from natural deposits in countries like China, New Zealand, America, Brazil and France. Halloysite nanotubes (HNTs) are a kind of two-layered aluminosilicate clay with chemical composition $Al_2Si_2O_5(OH)_4.2H_2O$, has a predominantly hollow micro and nanotubular structure chemically similar to kaolin group[11,12] and mostly used in the manufacturing of high quality ceramic white-ware and bone china[13]. HNTs are 1:1 phyllosilicates which are silicate sheet with six-member rings, consisting one tetrahedral sheet and one octahedral sheet. The physical appearance of HNTs is very similar to carbon nanotubes (CNTs), but the cost of HNTs is much lower. HNTs contain two types of hydroxyl groups, inner and outer hydroxyl groups, which are present between layers and on the surface of the nanotubes, respectively. The outer surface of HNTs is primarily composed of siloxane (Si –O-Si) groups, whereas the internal surface consists of a gibbsite-like array of aluminol (Al-OH) groups and less silanols/aluminols are present on the edges. The chemical properties of

halloysite outer surface are similar to SiO_2, while the properties of inner surface and edges of the tubes considered as Al_2O_3[14]. The zeta potential of HNTs is mostly negative at *p*H 6-7 due to the surface potential of SiO_2 with a small contribution from the positive Al_2O_3 inner surface[15]. Due to its multilayer structure, most of the hydroxyl groups are present in inner surface and a few on outer surfaces. Du *et al.*[16] reported that HNTs have an outer diameter of 10-50 nm, an inner diameter of 5-20 nm with 2-40 μm in length. HNTs are novel one dimension natural nanofillers with a unique combination of tubular nanostructure, large aspect ratio, natural availability, rich functionality, good biocompatibility, and high mechanical strength. These characteristics generate exceptional mechanical, thermal, and biological properties, are available at the low cost for HNTs/PNCs[17,18]. HNTs also show potential during the controlled release of active agents. So, HNTs may replace the more expensive CNTs in high-performance PNCs and multi-functional nanocomposites.

Ethylene vinyl acetate (EVA) is one of the important organic polymer, mostly used for electrical insulation, cable jacketing and repair, film for greenhouses, encapsulating materials for solar cell photo-voltaic modules and water proofing, footwear, corrosion protection and packaging of components. But, EVA alone does not fulfill the requirements of its thermal stability and mechanical properties in some definite areas. EVA is a random copolymer of ethylene and vinyl acetate (VA) monomers. VA content has two fundamental effects which influence the properties of EVA copolymers. The first effect is to disrupt the crystalline regions formed by the polyethylene segments of the copolymer and second effect is overriding of VA content results from the polar nature of the acetoxy side chain. The properties of EVA depend on the crystallinity of the EVA[19-22], is controlled by the VA content. Researchers found that increasing the polarity of the matrix, by increasing of the vinyl acetate content, improves its affinity towards the fillers[23]. For better dispersion of halloysite nanotubes in the polymeric matrix, the preparation of samples by solution casting is preferred than the melt mixing method of EVA matrix with HNTs filler. Many work has been performed on EVA-clay nanocomposites[24-27], in this paper we prepared EVA/HNTs nanocomposite with high (45 wt %) vinyl acetate content. The aim of this paper is to investigate the effect of the HNTs on the morphological, thermal and mechanical properties of EVA nanocomposites.

Experimental Section

Materials

Ethylene-vinyl acetate copolymer (EVM) with 45% vinyl acetate content (LEVAPREN 450), density 0.971gm/mL, and melt flow index 5g/min was supplied by Lanxess, India. Dicumyl peroxide (DCP, 99% pure) used as cross linking agent was obtained from Hercules, India. Halloysite nanotube was purchased from Sigma-Aldrich, Germany. This material had an average tube diameter of 50 nm and inner lumen diameter of 15 nm. Typical specific surface area of this halloysite was 65 m^2/g; pore volume of 1.25 mL/g; refractive index 1.54; and specific gravity 2.53 g/cm^3. The solvent toluene reagent grade (99%) was obtained from E. Merck (India) Ltd., Mumbai, India.

Preparation of EVA/HNTs nanocomposites

The EVA/HNTs nanocomposites were synthesized by solution casting technique. 10 parts of HNTs was dispersed in 100 parts of toluene, sonicated for 1 h and 10 parts of EVA was dissolved in 100 parts of toluene at room temperature (RT) for 1 h separately. The suspension with HNTs was added to the EVA solution and mixed again at RT for 1 h. DCP 1.2 phr as the curing agent was added to the solution. After stirring in toluene, it was sonicated for 0.5 h. The final solution was casted over teflon tray and kept for air drying followed by vacuum drying at 50°C till to get constant weight. The dried films were molded in a hot press at a pressure of 5 MPa at 160°C for an optimum cure time, determined from a Monsanto oscillating disc rheometer (ODR, 100S). The formulation of the samples is given in Table 1.

Characterization

The cure characteristics of the EVA/HNTs nanocomposites containing curing agent and HNTs was studied by Monsanto oscillating disc rheometer (ODR, 100S) at 160°C. The data obtained from Monsanto rheograph were minimum torque (M_L), maximum torque (M_H), cure time (t_{90}) and scorch time (t_{s2}). The curing rate index (CRI) was calculated by using the formula

Table 1 — Formulation for EVA/HNTs nanocompsites (phr)

Sample code	Ingredients		
	EVA	HNTs	DCP
EG_0	100	0	1.2
EH_1	100	2.5	1.2
EH_2	100	5	1.2
EH_3	100	7.5	1.2
EH_4	100	10	1.2

Curing rate index (CRI) = $\frac{100}{t_{90}-t_{s2}}$. The XRD analysis of HNTs and EVA/HNTs nanocomposites were performed by a Bruker D500 diffractometer to know the basal spacing of the halloysite nanotubes before and after mixing with EVA. The samples were scanned from 10-70^0 2θ for X-ray diffraction pattern (XRD) with Cu K_α (λ= 1.5418A^0) radiation operated at 40kV and 40mA in combination with a Ni filter. The basal spacing was calculated by using Bragg's law. Fourier transform infrared spectroscopy (FTIR, model Perkin Elmer RX-1 equipped with attenuated total reflectance (ATR) technique) was used to characterize the possible interaction between EVA and HNTs, in range between 450-4000 cm^{-1} with a 0.4 cm^{-1} resolution. HNTs were ground thoroughly with KBr at approximately 1-3% by mass and pressed into a pellet with a thickness of about 1mm. The surface morphology of EVA/HNTs nanocomposites were investigated by using scanning electron microscope (SEM) JEOL (JSM- 5900 LV) with an accelerating voltage of 20 kV. For conductivity, the fractured surfaces of frozen specimens in liquid nitrogen were gold coated before the observations. The mechanical properties of the nanocomposites with dumb bell shape specimens, punched out from the 2 mm thickness sheets obtained from the samples using a Wallace die cutter were carried out using universal testing machine (UTM, Hounsfield H10 KS). The tests were carried out as per ASTM D 412 standard at 25 ± 2°C with cross- head speed of 500 mm /min. Perkin-Elmer Pyris 6 TGA analyzer was used to study the decomposition of EVA/HNTs nanocomposites with heating rate 10°C/min under nitrogen atmosphere and in the temperature range of 30°C to 650°C. Dynamic mechanical properties were determined by using a dynamic mechanical analyzer (Perkin Elmer DMA7). The samples were subjected to a cyclic tensile strain with force amplitude of 0.1 N at frequency of 1 Hz at the rate of 2°C/min in the temperature range of -80°C to 140°C.

Results and Discussion

Curing characteristics

The curing characteristics of EVA/HNTs nanocomposites containing curing agent are listed in Table 2. It is observed that M_L, M_H, t_{90}, t_{s2} increases and CRI decreases marginally with the increase in HNTs loading in the nanocomposites. The increase may be due to the interaction of silanol and aluminol groups which are present on the surface as well as the edges of HNTs with the EVA matrix. The groups absorb the accelerators in the lumen of HNTs, which hinders the cross linking of polymer chains[28]. The increase in t_{90} and t_{s2} by adding 10 phr HNTs in natural rubber was reported by Rooj *et al.*[12]. Also the t_{90} of EPDM/HNTs nanocomposites increases with the increase in HNTs content (> 15 phr), reported by Ismail *et al.*[4]. As HNTs belong to kaolin group, which absorbs polymers through hydrogen bonding, acid-base interaction or charge transfer, etc.[28] The increase in M_H on addition of HNTs, non-deformable particles which restricts the polymer chain movement[29]. This may be also due to the strong intertubular and interfacial interaction between EVA and HNT, which reduces the EVA polymer chain mobility and thus increases the strength and stiffness of composites[30].

XRD analysis

Figure 1(inset) shows the X-ray diffraction pattern of the halloysite nanotubes. The peak at 11.9° 2Θ corresponds to (001) basal spacing of 0.748 nm, determined by Bragg's law. So it indicates that the halloysite was mainly in the dehydrated form and typically referred to as (7A°) halloysite. The basal reflections are broad and this is attributed to the small crystal size, the inconsistent layer spacing and curvature of the layers. The dehydrated state was also confirmed with the presence of the (001) basal reflection at 24.9° 2Θ, which equivalent to d=3.66A°. The relative sharp diffraction peak with d=1.72A° at 63.2° 2Θ, indicates that the halloysite is a dioctahedral mineral and this relates to the typical sheet structure of HNTs. It can also be seen that there

Table 2 — Curing characteristics of EVA/HNTs nanocomposites

Sample	Minimum rheometric torque, M_L (dN m)	Maximum rheometric torque ,M_H (dN m)	Rheometric scorch time, t_{s2} (min)	Rheometric cure time, t_{90} (min)	Curing rate index,CRI (min^{-1})
EG_0	3	27.5	0.5	25	4.1
EH_1	3.5	28	0.75	25.5	4.04
EH_2	3.5	28.5	0.75	26	3.96
EH_3	4	29	0.75	26.5	3.88
EH_4	4	30	1	27	3.84

are two other peaks at 22.5° 2Θ and 26.7° 2Θ, which corresponds to the presence of silica, in the forms of cristobalite and quartz, respectively.

XRD patterns of the HNTs, EVA/HNTs composites with loading 0 to 10 phr are represented in Fig. 1. Also the Table 3 presents the 2Θ° and their relative interlayer spacing at different basal reflection peaks. As illustrated in the Fig. 1 and Table 3 the (001) basal spacing of HNTs is increased from 0.748 nm to 0.756 nm, after mixing EVA and other ingredients with HNTs (2.5 phr). It was also observed that the (002) basal spacing of HNTs is expanded from 0.172 nm to 0.268 nm. Also adding 7.5 phr HNTs the basal spacing was increased to 0.786 nm, however further adding 10 phr it was decreased to 0.759 nm which is higher than halloysite.

FTIR analysis

The interactions between EVA matrix and filler HNTs were evaluated by the Fourier transforms infrared spectroscopy (FTIR) study and are represented in Fig. 2. The outer side of HNTs contains siloxanes and few Si-OH groups which are located in ends and surface defects, however with most of the Al-OH groups in the inner side. Hence, it is believed that there will be hydrogen bond formation between the silanol group of HNTs and acetate group of the EVA than that of the aluminols of HNTs. Therefore, the presence of silanol groups (Si-OH) can enhance the interfacial interaction between halloysite and polar polymers. HNTs show some obvious absorption bands at 437, 471 and 542 cm^{-1} due to deformation of Si-O, Si-O-Si and Al-O-Si respectively. The absorption bands around 912 cm^{-1} is assigned to the Al-OH vibrations. The bands at 1028 $cm^{-1}$and 1040 cm^{-1} in HNTs spectrum (Fig. 2a) are assigned to the Si-O stretching vibrations on HNTs surface[4]. The band at 1646 cm^{-1} is assigned to the O-H deformation vibration of adsorbed water. The interlayer H_2O band of HNTs was observed at 3565 cm^{-1}. The absorption bands at 3697 and 3655 cm^{-1} in HNTs spectrum are assigned to the O-H stretching of inner surface Al–OH groups, whereas band at 3627 cm^{-1} is assigned to the O-H stretching of inner Al–OH groups of HNTs. FTIR spectra of EVA/HNTs nanocomposites with 2.5 phr HNTs loading, the absorption peak of Al-OH and Si-O were shifted to 945 cm^{-1} and 1054 cm^{-1}, respectively. The shift is related to the formation of hydrogen bonding between the outer and inner surfaces OH groups of HNTs with acetate group of EVA. Further increasing the HNTs loading from 2.5 to 10 phr the absorption peaks the Si-O spectra

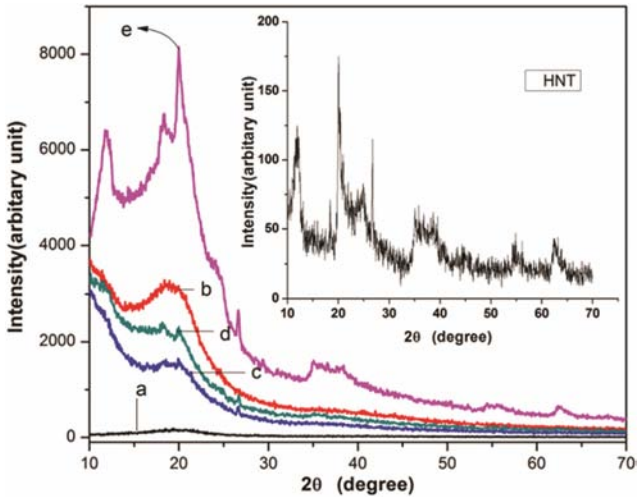

Fig. 1 — XRD pattern of (a) EVA/HNTs (0 phr) (b) EVA/HNTs (2.5 phr) (c) EVA/HNTs (5 phr) (d) EVA/HNTs (7.5 phr) (e) EVA/ HNTs (10 phr) nanocomposites.

Table 3 — XRD analysis of HNTs and EVA/HNTs nanocomposites

Sample	2θ (degree)	d (nm)
HNTs	11.9	0.748
EG_0	19.4	0.246
EH_1	11.85	0.756
EH_2	11.75	0.759
EH_3	11.3	0.786
EH_4	11.75	0.759

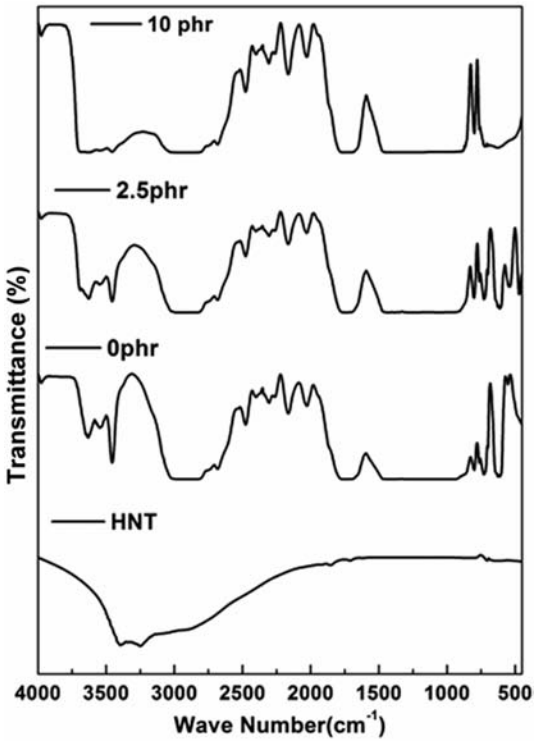

Fig. 2 — FTIR spectra of HNTs and EVA/HNTs nanocomposites

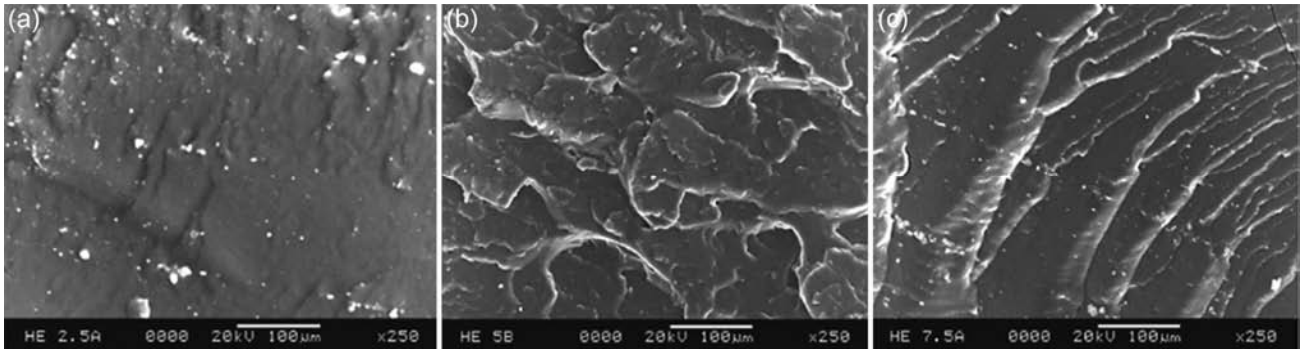

Fig. 3 — SEM images cryogenically fractured EVA/HNTs nanocomposites (a) 2.5 phr (b) 5.0 phr (c) 7.5 phr HNTs.

again appear at 1027 cm^{-1}, which indicates the poor interaction of polymer and HNTs at higher loading. Du *et al.*[28] also used FTIR to characterize the formation of hydrogen bonding between carboxylated butadiene-styrene and HNTs. For EVA nanocomposite without HNTs the C-H stretching vibration of acetate group was observed around 2853 cm^{-1}. The peaks around 3630 and 3629 cm^{-1} of 2.5 and 10 phr HNTs loaded nanocomposites indicates the interaction of OH groups of HNTs with EVA matrix at different extent[31]. FTIR absorption bands around 2858 cm^{-1} and 2842 cm^{-1} for 2.5 phr and 10 phr HNTs loading nanocomposites was due to the C-H stretching vibration. Since most of the aluminol (Al-OH) groups are present in the inner side of the HNTs crystalline structure, the absorptions shifts for aluminols are much less than that of the Si-O. It is thought that the shifts of FTIR absorption peaks are due to the formation of hydrogen bonds of the hydroxyl groups and the Si-O groups on the surface of HNTs with the acetate group of EVA.

Scanning electron microscopy (SEM) analysis

The SEM images of cryogenically fractured EVA/HNTs nanocomposites are shown in Fig. 3. The roughness of the fracture surface increased with the increase in HNTs loading. Fig. 3(a) and Fig.3(b) show that the HNTs are uniformly distributed in the EVA matrix upto 5 phr loading, which suggests strong interfacial interaction, reflected in the tensile strength of the nanocomposites. Fig. 3(c) shows that at 7.5 phr HNTs loading results in agglomeration of filter particles due to dominance of strong HNTs-HNTs interaction over EVA-HNT interaction. The interfaces between HNTs and EVA are clear and many debonded nanotubes pulled out from matrix at higher filler loading.

Mechanical properties

The effect of HNTs loading on tensile strength of EVA/HNTs nanocomposites was shown in Fig. 4a.

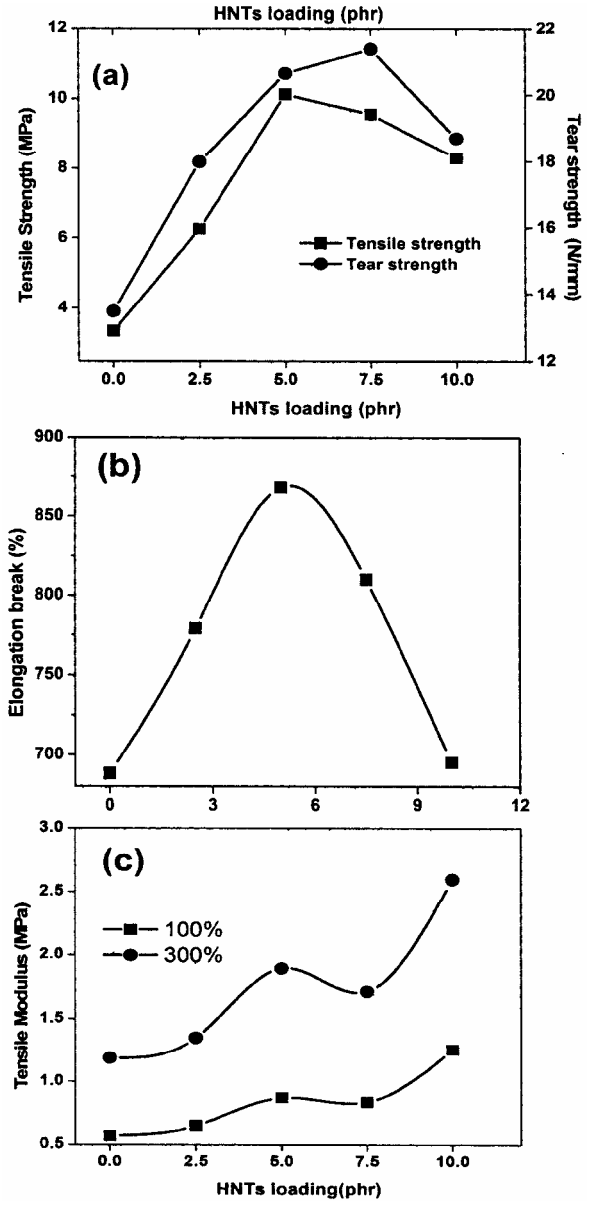

Fig. 4 — Mechanical properties (a) Tensile and Tear strength (b) Elongation at break and (c) Stress at 100% and 300% elongation of EVA/HNTs nanocomposites as a function of HNT loading.

The optimum tensile strength was obtained at 5 phr HNTs loading due to good dispersion of HNTs into the EVA matrix. The increment in tensile strength of EVA/HNTs nanocomposites, especially at 5 phr HNTs loading can be attributed to factors such as uniform distribution of HNTs inside the EVA, strong interfacial and intertubular interaction between HNTs and EVA matrix. The good dispersion of HNTs into the EVA matrix is validated by SEM analysis. However with further increase in HNT loading the tensile strength gradually decreased but higher than EVA gum. This decrease in tensile strength at higher HNTs concentration (7.5-10 phr) is due to the dominance of filler-filler interaction than the filler-polymer interaction, which results in agglomeration of the filler particles, can be seen in the SEM images (Fig. 3). However, the tear strength of EVA/HNTs nanocomposites increases up to 7.5 phr HNTs loading (Fig. 4a). Elongation at break (E_b) of the EVA/HNTs nanocomposites at different HNTs loading is represented in Fig. 4b. It is observed that the E_b of nanocomposites increases with increase in HNTs loading up to 5 phr and afterwards, it decreases with higher HNTs loading. The behaviour of these composites towards E_b is due to the simultaneous increase of ductility and stiffness of nanocomposites with the increase in HNTs content up to 5 phr and afterwards, at higher filler loading, the ductility becomes worst which restricts the molecular chains movement[32]. The decrease in E_b may be due to the agglomeration due to filler-filler interaction. The effect of HNTs loading on the tensile modulus at 100% and 300% (M100 and M300) of EVA/HNTs nanocomposites are shown in Fig. 4c. The M100 and M300 also show an increasing trend up to 5 phr and decrease on 7.5 phr HNTs loading. The enhancement of property related to the strong interaction between EVA and HNTs.

Thermogravimetric analysis (TGA)

Figure 5(a) shows the TGA curves of EVA/HNTs nanocomposites with 0-10 phr HNTs loading, where as Table 4 shows the results of thermal properties of these nanocomposites. Thermal stability of nanocomposites enhanced as compared to unfilled EVA/HNTs nanocomposites due to the formation of

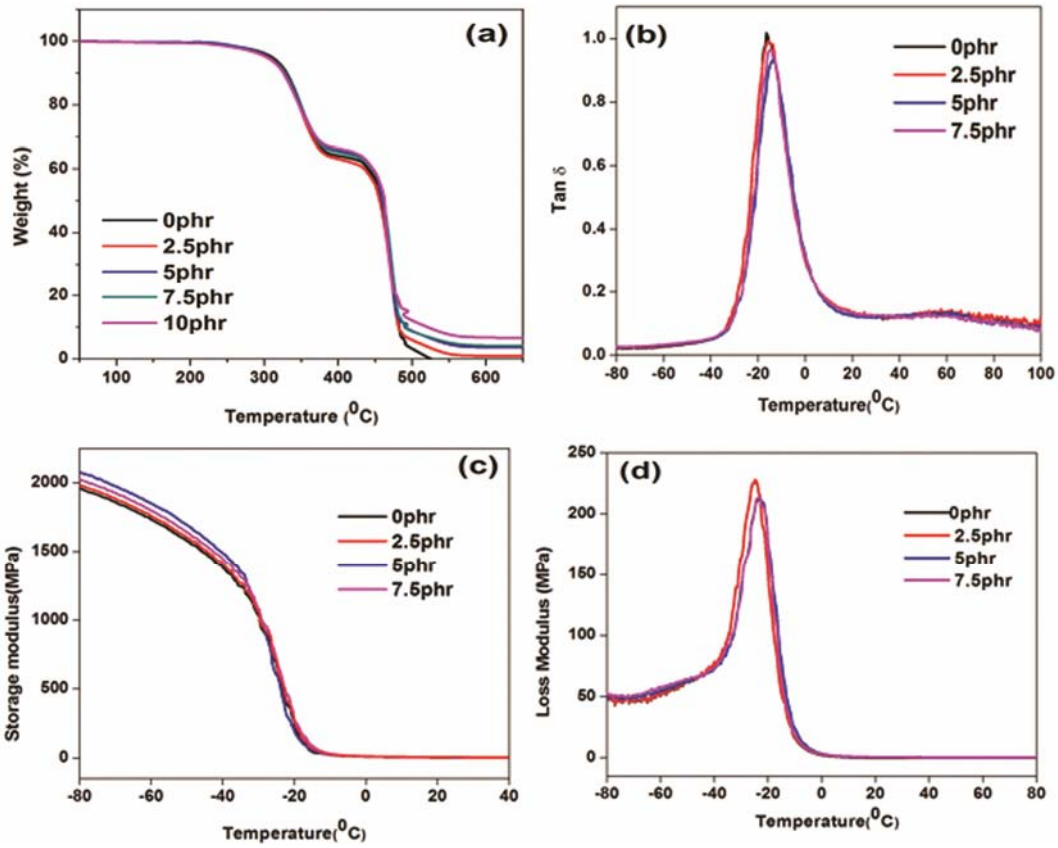

Fig. 5 — TGA/DMA curves of EVA/HNTs nanocomposites (a) TGA (b) temperature dependence of tan δ (c) temperature dependence of storage modulus (d) temperature dependence of loss modulus.

Table 4 — Thermal stability parameters of EVA-HNTs nanocomposites

HNTs loading (phr)	Temperature at 5% mass loss	Temperature at 50% mass loss	Maximum mass loss(%)	Temperature (°C) at maxium mass loss
0	310	459	99	517
2.5	306	456	99	580
5	305	459	96	564
7.5	305	461	96	595
10	304	463	93.3	597

hydrogen bonding between the silanol and siloxane groups present on the surface of HNTs and vinyl acetate group of EVA. The thermal degradation temperature of EVA undergoes two stages. The first stage is attributed to the elimination of acetic acid, which occurs at about the temperature between 300-400°C and the second stage is the main-chain degradation of the polymer. At the first step, the degradation of EVA/HNTs nanocomposites became faster than that of the pure EVA. This can be assigned to the loss of acetic acid which was accelerated as a function of HNTs loading, which is almost consistent with the result of Lee *et al.*[33], who reported EVA40/organoclay nanocomposites. The temperature at 5% mass loss was decreased with the increase in HNTs loading; however the 50% mass loss was increased. Table 4 also shows the decrease in maximum mass losses of EVA/HNTs nanocomposites with the increase in filler loading from 0-10 phr. It reveals that the char residue of nanocomposites increase in comparison to the EVA matrix and it also increases with the increase in HNTs loading in EVA/HNTs nanocomposites. This char residue on the surface of the nanocomposites exposed to heat and protects the samples from heat[34]. Many authors also reported that the formation of char can protect the volatile decomposition products[4,8,34,35]. HNTs can acts as thermal barrier properties which also delay the mass loss by entrapping the elastomers into their lumen structure as reported by Du *et al.*[16] who reported that the degradation products of polypropylene may be entrapped inside the lumens of HNTs, remarkably increased thermal stability of PP/HNTs nanocomposites.

It is also reported by many researchers[36-38] that the best thermal stability of nanocomposites obtained for clay filled PNCs with 6-8 phr filler content, which was attributed to the well-dispersed nanoparticles at low clay content and exfoliation. HNTs which are a phyllosilicate group as MMT, expected to show similar behaviour.

Table 5 — The effect of HNTs loading on the tan δ and storage modulus (E′) of EVA/HNTs nanocomposites at 25°C.

HNTs loading (phr)	Tan δ	Storage modulus,E′ (MPa)
0	0.133	3.12
2.5	0.131	3.92
5	0.119	4.51
7.5	0.125	4.18

Dynamic mechanical analysis (DMA)

The tan δ, storage modulus (E′) and loss modulus (E″) were measured to analyze the polymer- filler interaction in the EVA/HNTs nanocomposites. Figure 5(b) to Fig. 5 (d) show the effect of HNTs loading on tan δ, storage modulus (E′) and loss modulus (E″) of EVA/HNTs nanocomposites at different temperatures. The value of tan δ is the ratio between the energy of dissipation to energy stored per cycle which measures the elasticity of a material (as elasticity is inversely proportional to tan δ). The peak of tan δ vs temperature curve is taken as the glass transition temperature (T_g). Figure 5(b) shows that the T_g of the EVA/HNTs nanocomposites increases slightly with HNTs loading up to 5 phr and then decreases above 5 phr HNTs loading. The increase in Tg of nanocomposites may be due to decrease in the segmental motion of the elastomeric chains. The addition of HNTs shows the decrease of tan δ_{max} (tan δ value at Tg). The tan δ_{max} value of nanocomposites decreases up to 5 phr HNTs loading and then increases which may be due to filler-filler interaction at higher HNTs loading. The tan δ values of EVA/HNTs nanocomposites at 25°C were listed in Table 5.

Generally, higher storage modulus and lower tan δ value shift of the glass transition temperature (T_g) to higher temperature which attributes to the stronger interactions between the elastomer and filler[39]. Figure 5(c) shows the increase in storage modulus (E′) of EVA/HNTs nanocomposites up to 5 phr HNTs loading and decreases at higher HNTs loading. The storage modulus of all the EVA/HNTs nanocomposites is found to be higher than the EVA matrix (Table 5). The increasing of storage modulus indicates the strong interfacial and intertubular interaction between EVA and HNTs at lower filler loading; however it decreases on higher filler loading due to the agglomeration of HNTs nanoparticles. Figure 5(d) shows the temperature of maximum loss modulus (E″) is very close to the T_g of nanocomposites.

Conclusion

EVA/HNTs nanocomposites have been prepared with 0 to 10 phr loading of HNTs by solution casting method. The M_H, t_{90} ,and t_{s2} increases while the CRI decreases marginally with the increase in HNTs loading in the nanocomposites. XRD analysis indicates the intercalation of HNTs in EVA matrix. FTIR studies shows there is a good interaction between the EVA matrix and HNTs filler due to the dispersion of HNTs in matrix. The optimum tensile strength and elongation at break could be achieved at 5 phr HNTs loading and then decreases at higher HNTs loading, due to the poor dispersion and agglomeration of HNTs at higher loading. The optimum tear strength is achieved at 7.5 phr HNTs loading and decreases at higher filler loading. The tensile modulus at 100% and 300% elongation of nanocomposites increase up to 5 phr HNTs loading and thereafter, it decreases at higher HNTs loading. HNTs filled EVA nanocomposites show good thermal stability due to the entrapment of degradation products of EVA inside the lumen structure of HNTs. DMA analysis shows that the storage modulus and T_g of the nanocomposites increases with the addition of HNTs and however at higher loading it decreases as HNTs agglomerates.

Acknowledgement

The authors thank Lanxess India, for kindly supplying the LEVAPREN 450 used in this study.

References

1 Ray S S & Okamoto M , *Prog Polym Sci*, 28(2003) 1539.
2 Arayapranee W & Rempel G L, *J Appl Polym Sci*, 109 (2008) 932.
3 Pasbakhsh P, Ismail H, Ahmad Fauzi M N & Abu Bakar A, *J Appl Polym Sci*, 113 (2009) 3910.
4 Ismail H, Pasbakhsh P, Ahmad Fauzi M N & Abu Bakar A, *Polym Test*, 27 (2008) 841.
5 Arroyo M, Lopez-Manchado M A & Herrero B, *Polym*, 44 (2003) 2447.
6 Teh P L, Mohd Ishak Z A, Hashim A S, Karger-Kocsis J & Ishiaku U S, *J Appl Polym Sci*, 94 (2004) 2438.
7 Tang B X, Shi J H, Pramota K P & Goh S H , *Nanotechnol*, 18 (2007) 125606.
8 Munusamy Y, Ismail H & Mariatti M, *J Rein Plas Com*, 27(2008) 1925.
9 Moniruzzaman M & Winey K I, *Macromol*, 39 (2006) 5194.
10 Byrne M T & Gun'ko Y K, *Adv Mater*, 22 (2010) 1672.
11 Liu M, Guo B, Lei Y, Du M, Cai X & Jia D, *Nanotechnol*, 18 (2007) 455703.
12 Rooj S, Das A, Thakur V, Mahaling R N, Bhowmick A K & Heinrich G , *Mater Design*, 31 (2010) 2151.
13 Bates T F, Hildebrand F A & Swineford A, *Am Mineral*, 35 (1950) 463.
14 Shchukin D G, Sukhorukov G B, Price R R & Lvov Y M, *Small*, 1 (2005) 510.
15 Tari G, Bobos I , Gomes CSF & Ferreira J M F, *J Colloid Interf Sci*, 210 (1999) 360.
16 Du M, Guo B & Jia D, *Eur Polym J*, 42 (2006) 1361.
17 Du M, Guo B & Jia D, *Polym Int*, 59 (2010) 574.
18 Lvov Y & Abdullayev E, *Prog Polym Sci*, 38 (2013) 1690.
19 Brogly M, Nardin M & Schultz J, *J Appl Polym Sci*, 64 (1997) 1903.
20 Arsac A, Carrot C & Guillet J, *J Appl Polym Sci*, 74 (1999) 2625.
21 Bistac S, Kunemann P & Schultz J, *Polymer*, 39 (1998) 4875.
22 Gospodinova N, Zlatkov T & Terlemezyan L, *Polymer*, 39 (1998) 2583.
23 Miltner H E, Peeterbroeck S, Viville P, Dubois P & Van Mele B, *J Polym Sci :B Pol Phys*, 45 (2007) 1291.
24 Padhi S, Achary P G R & Nayak N C, *Bull Mater Sci*, 38 (2015) 925.
25 Aghjeh M R, Mardani E, Rafiee F, Otadi M, Khonakdar H A, Jafari H S & Reuter U, *Polym Bull*, (2016) 1.
26 Aghjeha M R, Asadi V, Mehdijabbar P, Khonakdar H A & Jafari H S, *Composites Part B: Eng*, 86 (2016) 273.
27 Li X & Ha C S, *J Appl Polym Sci*, 87 (2003) 1901.
28 Du M, Guo B, Lei Y, Liu M & Jia D, *Polymer*, 49 (2008) 4871.
29 Ismail H, *J Elast Plas*, 33 (2001) 34.
30 Ismail H, Pasbakhsh P, Ahmad Fauzi M N, Abu Bakar A, *Polym-Plas Tech Eng*, 48 (2009) 313.
31 Pal P, Kundu M K, Kalra S & Das C K, *Open J Appl Sci*, 2 (2012) 277.
32 Osabohien E & Egboh S H O, *J Appl Polym Sci*, 107 (2008) 210.
33 Lee H M, Park B J, Gupta R K, Bhattachary S N & Choi H J, *J Macrom Sci Part B: Phys,* 46 (2007) 261.
34 Zhu J, Morgan AB, Lamelas F J & Wilkie C A, *Chem Mater*, 13 (2001) 3774.
35 Kotsilkova R, Petkova V & Pelovski Y, *J Therm Anal Calorim*, 64 (2001) 591.
36 Leszczynska A, Njuguna J, Pielichowski K & Banerjee J R, *Thermochemi Acta*, 453 (2007) 75.
37 Lim S T, Hyun Y H, Choi H J & John M S, *Chem Mater*, 14 (2002) 1839.
38 Ahmadi S J, Huang Y & Li W, *Compos Sci Technol*, 65 (2005) 1069.
39 López-Manchado M A, Herrero B & Arroyo M, *Polym Int* , 53 (2004) 1766.